

## DISCOVERY OF THE NEW X-RAY TRANSIENT MAXI J1807+132: A CANDIDATE OF A NEUTRON STAR LOW-MASS X-RAY BINARY

MEGUMI SHIDATSU,<sup>1</sup> YUTARO TACHIBANA,<sup>2</sup> TAKETOSHI YOSHII,<sup>2</sup> HITOSHI NEGORO,<sup>3</sup> TAIKI KAWAMURO,<sup>4</sup> WATARU IWAKIRI,<sup>1</sup>  
SATOSHI NAKAHIRA,<sup>1</sup> KAZUO MAKISHIMA,<sup>1</sup> YOSHIHIRO UEDA,<sup>4</sup> NOBUYUKI KAWAI,<sup>2</sup> MOTOKO SERINO,<sup>1</sup> AND JAMIE KENNEA<sup>5</sup>

<sup>1</sup>*MAXI team, RIKEN, 2-1 Hirosawa, Wako, Saitama 351-0198, JAPAN*

<sup>2</sup>*Department of Physics, Tokyo Institute of Technology, 2-12-1 Ookayama, Meguro-ku, Tokyo 152-8551*

<sup>3</sup>*Department of Physics, Nihon University, 1-8-14 Kanda-Surugadai, Chiyoda-ku, Tokyo 101-8308, Japan*

<sup>4</sup>*Department of Astronomy, Kyoto University, Kitashirakawa-Oiwake-cho, Sakyo-ku, Kyoto, Kyoto 606-8502, Japan*

<sup>5</sup>*Department of Astronomy and Astrophysics, 0525 Davey Laboratory, Pennsylvania State University, University Park, PA 16802, USA*

### ABSTRACT

We report on the detection and follow-up multi-wavelength observations of the new X-ray transient MAXI J1807+132 with the MAXI/GSC, *Swift*, and ground-based optical telescopes. The source was first recognized with the MAXI/GSC on 2017 March 13. About a week later, it reached the maximum intensity ( $\sim 10$  mCrab in 2–10 keV), and then gradually faded in  $\sim 10$  days by more than one order of magnitude. Time-averaged *Swift*/XRT spectra in the decaying phase can be described by a blackbody with a relatively low temperature (0.1–0.5 keV), plus a hard power-law component with a photon index of  $\sim 2$ . These spectral properties are similar to those of neutron star low-mass X-ray binaries (LMXBs) in their dim periods. The blackbody temperature and the radius of the emission region varied in a complex manner as the source became dimmer. The source was detected in the optical wavelength on March 27–31 as well. The optical flux decreased monotonically as the X-ray flux decayed. The correlation between the X-ray and optical fluxes is found to be consistent with those of known neutron star LMXBs, supporting the idea that the source is likely to be a transient neutron star LMXB.

*Keywords:* X-rays: individual (MAXI J1807+132) — X-rays: binaries

## 1. INTRODUCTION

Many of X-ray point sources in the sky have significant variability on various timescales. In particular, transient low-mass X-ray binaries (LMXBs), involving accreting neutron stars or black holes, exhibit dramatic outbursts, changing their X-ray luminosity by orders of magnitude in relatively short periods (a few days to months; see e.g., Done et al. 2007, for a review). Because their luminosity is mainly determined by the mass accretion rate, their transient nature makes them ideal objects to study the physics of accretion onto compact objects over a wide range of mass accretion rates.

The new transient MAXI J1807+132, located at an off-Galactic-plane region with a Galactic latitude of  $15^\circ.5$ , was first noticed on 2017 March 13 (Negoro et al. 2017) by the nova-search system (Negoro et al. 2016) of the Monitor of All-sky X-ray Image (MAXI; Matsuoka et al. 2009), in an X-ray image provided by the MAXI/Gas Slit Camera (GSC; Mihara et al. 2011). The source position estimated with the MAXI/GSC turned out to be consistent with that of 2MAXIt J1807+132, which is listed in the MAXI/GSC transient source catalog (Kawamuro et al. 2016), based on an X-ray flaring event detected in 2011 May.

As shown in Figure 1, the source was detected in a 7-tile follow-up observation with the *Swift*/X-ray Telescope (XRT; Gehrels et al. 2005), and Ultra-Violet and Optical Telescope (UVOT; Roming et al. 2005), in the X-ray band and the optical to ultraviolet bands, respectively. Thus, the source position was determined accurately as  $(\alpha^{2000}, \delta^{2000}) = (18^{\text{h}}08^{\text{m}}07^{\text{s}}.549, +13^\circ15'05.''40)$  and  $(l, b) = (40^\circ.123127, 15^\circ.501653)$  with a 90 % uncertainty of  $0.''16$  (Kennea et al. 2017a,b). The UVOT  $u$ ,  $b$ , and  $v$ -band magnitudes were  $17.4 \pm 0.1$  mag,  $18.4 \pm 0.2$  mag, and  $>17.6$  mag at that time (Kennea et al. 2017b), respectively. The source was also followed by ground-based optical telescopes (Shields et al. 2017; Tachibana et al. 2017a; Muñoz-Darias et al. 2017; Armas Padilla et al. 2017a; Kong et al. 2017).

These follow-up X-ray and optical observations have provided pieces of information to understand the nature of the object. The source showed significant flux variations in the optical band (Shields et al. 2017; Tachibana et al. 2017a; Armas Padilla et al. 2017a; Kong et al. 2017) as well as X-rays (Negoro et al. 2017; Armas Padilla et al. 2017a; Kong et al. 2017). Denisenko (2017) recognized the optical counterpart in an image taken about 35 years ago and suggested past activities of the source. The source was also detected optically in PanSTARRS-1 multi-epoch data, with a magnitude which was larger by 2–3 (i.e.,  $\sim 10$ )

times fainter in terms of the flux) than those obtained 35 years ago and in 2017 March (Denisenko 2017). LMXB-like characteristics were found through preliminary modeling of the XRT spectra (Shidatsu et al. 2017) and optical spectroscopy (Muñoz-Darias et al. 2017).

In this paper, we present the first results from the multi-wavelength monitoring of MAXI J1807+132 in 2017 March and April, with the MAXI/GSC, *Swift* and ground-based optical telescopes, and discuss the nature of the source. Throughout the paper, errors represent the 90% confidence intervals of a single parameter with  $\Delta\chi^2 = 2.706$ , unless otherwise stated.

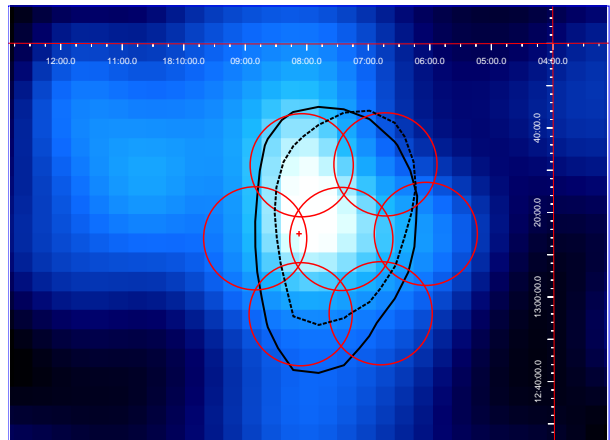


**Figure 1.** A 2–4 keV image ( $2^\circ.3 \times 1^\circ.7$ ) obtained in the MAXI/GSC observation from 2017 March 13 to April 1. The thick solid and dashed lines (black) indicate the error regions of MAXI J1807+132 determined by the MAXI/GSC in the 2–4 keV and 4–10 keV bands, respectively. The seven red circles represent the fields-of-view of the *Swift*/XRT for individual pointings on March 26. The red cross point indicates the position of the source detected with *Swift*.

## 2. X-RAY OBSERVATIONS AND RESULTS

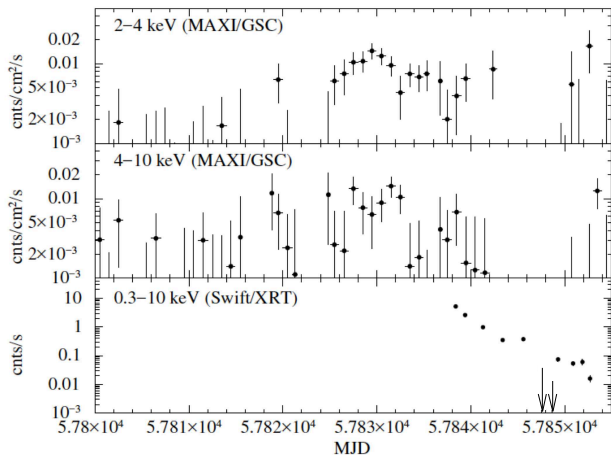
### 2.1. Long-term Monitoring with MAXI

After the first detection on 2017 March 13, MAXI J1807+132 has been monitored with the MAXI/GSC. Figure 2 presents background-subtracted 2–4 keV and 4–10 keV light curves, created through the method of image fitting (Morii et al. 2016) to the MAXI/GSC event data version 1.8. The source intensity reached a maximum at around MJD 57827–MJD 57832 (2017 March 15–20), and then gradually decreased. The averaged 4–10 keV intensity was  $\approx 9$  mCrab in that period, which is comparable with the peak intensity of the X-ray flaring event from 2MAXIt J1807+132 recorded in Kawamuro et al. (2016).

### 2.2. *Swift*/XRT Spectral Analysis

**Table 1.** Log of *Swift*/XRT observations

Date	Start time (UT)	End time (UT)	Net exposure (ks)	XRT mode <sup>a</sup>
2017 Mar 26	08:44:23	10:26:52	0.22	PC
2017 Mar 27	07:01:39	09:50:56	1.94	WT
2017 Mar 29	05:08:51	07:01:38	1.99	WT
2017 Mar 31	08:13:39	11:12:56	2.05	WT
2017 Apr 02	14:18:11	14:29:56	0.69	WT
2017 Apr 04	11:06:57	11:07:02	0.005	WT
2017 Apr 05	15:36:52	15:52:53	0.95	PC
2017 Apr 06	06:08:03	06:16:52	0.51	PC
2017 Apr 07	21:38:20	21:54:53	0.98	PC
2017 Apr 08	21:29:20	21:44:53	0.91	PC
2017 Apr 09	16:56:20	17:12:53	0.99	PC

<sup>a</sup>PC and WT indicate the Photon Counting mode and the Windowed Timing mode, respectively.**Figure 2.** MAXI/GSC light curves in 2–4 keV (top) and 4–10 keV (middle) with one-day time bins, and *Swift*/XRT light curve in 0.3–10 keV (bottom), with one observation per bin. The arrows represent upper limits. MJD 57825 corresponds to 2017 March 13.

A series of follow-up pointed observations of MAXI J1807+132 were carried out with *Swift* in the decaying phase. The net exposure was 0.5–2 ks in each observation. A log of these observations is given in Table 1, and the 0.3–10 keV XRT light curve is shown in Figure 2. We analyzed the XRT spectra taken during two weeks from the first *Swift* observation (March 26), using XSPEC version 12.9.1m (Arnaud 1996). The light

curve, spectra, and responses were downloaded via the online tools provided by the UK Swift Science Data Centre (Evans et al. 2009)<sup>1</sup>. The spectra taken on March 27 and March 29, which have the best statistics among the present XRT datasets, were binned so that at least 30 counts are contained in each bin, and were analyzed on the basis of the  $\chi^2$  statistics. The other data, which have lower statistics, were grouped so that each bin has at least one count, and the Cash-statistics (Cash 1979) were adopted in the spectral analysis. The data taken on April 4 and 5 were omitted, because the source was not detected significantly. The data on April 6 and 7 were merged together to improve statistics; so were those on April 8 and 9. In the following analysis, the TBabs model is employed as the interstellar absorption model, with the table of solar abundances provided by Wilms et al. (2000).

As shown in Figure 3, we first analyzed the XRT spectra on March 27 and 31, which were obtained when the source intensity was relatively high and low, respectively. The spectrum on March 27 can be fit with an absorbed power-law model with a photon index of  $\Gamma = 2.4^{+0.2}_{-0.1}$  and a column density of  $N_{\text{H}} = (2.5 \pm 0.6) \times 10^{21} \text{ cm}^{-2}$ , in agreement with the first report by Kennea et al. (2017a,b). This model is fully acceptable (Fig. 3b), with  $\chi^2/\text{dof} = 63/65$ . The resultant parameters are listed in Table 1. However, the estimated column density is somewhat higher than the total Galactic column,  $N_{\text{H}} = 1.0 \times 10^{21} \text{ cm}^{-2}$  derived using the tool `nh` in HEASOFT version 6.19, and that calculated from the optical spectrum of the source ( $N_{\text{H}} \sim 1.6 \times 10^{21} \text{ cm}^{-2}$ ; Muñoz-Darias et al. 2017). The fit quality became worse ( $\chi^2/\text{dof} = 84/66$ ), when  $N_{\text{H}}$  is fixed at  $1.0 \times 10^{21} \text{ cm}^{-2}$  (Fig. 3c).

As observed in Figure 3(a), the XRT spectrum changed significantly in shape from March 27 to March 31. The March 31 spectrum appears to consist of a softer component dominant in  $< 2 \text{ keV}$ , and a harder power-law-like component with a photon index of  $\leq 2$  extending above 2 keV. Then, the spectral change from March 27 to 31 can be understood if the latter component decreased by an order of magnitude, with a relatively small change in the former. As a confirmation, we forced a single power-law model to the March 31 spectrum. The fit was formally acceptable (Table 1), but as shown in Figure 3(e), the data in  $> 2 \text{ keV}$  systematically exceeded the best-fit power-law model, which was required to have a very steep ( $\Gamma \sim$

<sup>1</sup> [http://www.swift.ac.uk/user\\_objects/](http://www.swift.ac.uk/user_objects/)

**Table 1.** Best-fit parameters of various spectral models for the *Swift*/XRT data on March 27 and 31

Parameter	$N_{\text{H}}$	$\Gamma$ or $\tau$	$N_{\text{pl}}^{\text{a}}$	$R_{\text{bb (comp)}}^{\text{b}}$	$kT_{\text{bb}}$ or $kT_{\text{in}}$	$R_{\text{bb}}$ or $R_{\text{in}}^{\text{c}}$	$F_{\text{X}}^{\text{d}}$	$\chi^2/\text{dof}^{\text{e}}$
Unit	$10^{21} \text{ cm}^{-2}$			km	keV	km	$\text{erg s}^{-1} \text{ cm}^{-2}$	
<b>Model: TBabs*powerlaw</b>								
Mar. 27	$2.5 \pm 0.6$	$2.4^{+0.2}_{-0.1}$	$12 \pm 1$	-	-	-	$5.7 \times 10^{-11}$	63/65
Mar. 27	1.0 (fixed)	$2.07 \pm 0.07$	$8.4 \pm 0.4$	-	-	-	$4.6 \times 10^{-11}$	84/66
Mar. 31	$< 1.3$	$3.2^{+1.0}_{-0.4}$	$0.7^{+0.4}_{-0.1}$	-	-	-	$3.9 \times 10^{-12}$	19/18
Mar. 31	1.0 (fixed)	$3.9 \pm 0.5$	$1.0 \pm 0.2$	-	-	-	$8.2 \times 10^{-12}$	21/19
<b>Model: TBabs*(diskbb+powerlaw)</b>								
Mar. 27	1.0 (fixed)	$1.6^{+0.3}_{-0.7}$	$3 \pm 2$	-	$0.50^{+0.09}_{-0.06}$	$1.8^{+0.3}_{-0.7}$	$4.1 \times 10^{-11}$	60/64
Mar. 31	1.0 (fixed)	$1.4^{+1.0}_{-1.3}$	$0.2^{+0.3}_{-0.1}$	-	$0.15 \pm 0.03$	$19^{+17}_{-9}$	$7.8 \times 10^{-12}$	10/17
<b>Model: TBabs*(bbodyrad+powerlaw)</b>								
Mar. 27	1.0 (fixed)	$1.8 \pm 0.2$	$5 \pm 1$	-	$0.32^{+0.06}_{-0.04}$	$4.2^{+1.6}_{-1.5}$	$4.1 \times 10^{-11}$	59/64
Mar. 31	1.0 (fixed)	$1.5 \pm 1.0$	$0.2^{+0.3}_{-0.1}$	-	$0.12 \pm 0.02$	$32^{+22}_{-12}$	$7.2 \times 10^{-12}$	10/17
<b>Model: TBabs*(bbodyrad+compps(bbodyrad))</b>								
Mar. 27 <sup>f</sup>	1.0 (fixed)	$2.5^{+0.5}_{-0.4} \text{ }^{\text{h}}$	-	$18^{+1}_{-3}$	$0.22 \pm 0.05$	$< 10$	$3.7 \times 10^{-11}$	62/64
Mar. 27 <sup>g</sup>	1.0 (fixed)	$0.59^{+0.08}_{-0.07}$	-	$12.9^{+0.2}_{-1.7}$	$0.26 \pm 0.03$	$< 6$	$3.8 \times 10^{-11}$	64/64
Mar. 31 <sup>f</sup>	1.0 (fixed)	$3.0^{+0.0}_{-1.2} \text{ }^{\text{h}}$	-	$7 \pm 0.2$	$0.11 \pm 0.02$	$33^{+21}_{-12}$	$6.3 \times 10^{-12}$	10/17
Mar. 31 <sup>g</sup>	1.0 (fixed)	$1.5^{+1.5}_{-1.3} \text{ }^{\text{h}}$	-	$7 \pm 0.2$	$0.12 \pm 0.02$	$30^{+20}_{-9}$	$6.4 \times 10^{-12}$	10/17
<b>Model: TBabs*(diskbb+compps(diskbb))</b>								
Mar. 27 <sup>f</sup>	1.0 (fixed)	$3.0^{+0.0}_{-0.8} \text{ }^{\text{h}}$	-	$1.1^{+0.3}_{-0.1}$	$0.41^{+0.07}_{-0.12}$	$< 2.9$	$3.9 \times 10^{-11}$	60/64
Mar. 27 <sup>g</sup>	1.0 (fixed)	$0.7^{+2.3}_{-0.3} \text{ }^{\text{h}}$	-	$1.2 \pm 0.2$	$0.44^{+0.10}_{-0.08}$	$< 2.5$	$4.0 \times 10^{-11}$	59/64
Mar. 31 <sup>f</sup>	1.0 (fixed)	$3.0^{+0.0}_{-1.1} \text{ }^{\text{h}}$	-	$2.0^{+0.7}_{-0.2}$	$0.14 \pm 0.03$	$20^{+12}_{-9}$	$6.8 \times 10^{-12}$	11/17
Mar. 31 <sup>g</sup>	1.0 (fixed)	$2.0^{+1.0}_{-1.7} \text{ }^{\text{h}}$	-	$1.8^{+0.7}_{-0.4}$	$0.15 \pm 0.03$	$17^{+16}_{-8}$	$6.9 \times 10^{-12}$	10/17

<sup>a</sup>Normalization of the power-law component, in units of  $10^{-3}$  photons  $\text{keV cm}^{-2}$

<sup>b</sup>Radius of the emission region of the seed photons for Compton scattering, calculated from the photon flux of the **compps** component in 0.8–100 keV, by assuming a distance of 5 kpc and a spherical corona.

<sup>c</sup>The radius of emission region for the **bbodyrad** component, or the inner disk radius for the **diskbb** component. The distance and the inclination angle are assumed as 5 kpc and  $0^\circ$ , respectively.

<sup>d</sup>The unabsorbed X-ray flux in the 0.3–10 keV band.

<sup>e</sup>C-statistic/dof is instead presented for the March 31 results.

<sup>f</sup> $kT_e = 20$  keV is assumed.

<sup>g</sup> $kT_e = 100$  keV is assumed.

<sup>h</sup>The upper limit is pegged.

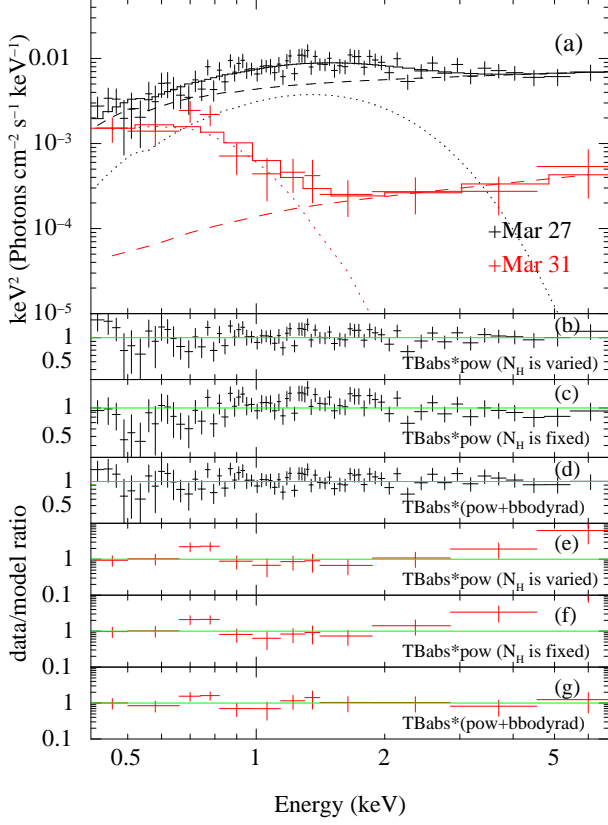


**Figure 3.** (a) Time-averaged *Swift*/XRT spectra on March 27 (black) and 31 (red) in the  $\nu F_\nu$  form, with their best-fit TBabs\*(powerlaw+bbodyrad) models. The contributions of the powerlaw and bbodyrad components are also shown separately in the dashed and dotted lines, respectively. (b) The March 27 data divided by the TBabs\*(powerlaw) model with free  $N_H$ , (c) by that with  $N_H = 1 \times 10^{21} \text{ cm}^{-2}$  (fixed), and (d) divided by the TBabs\*(powerlaw+bbodyrad) model. (e)–(g) The same as (b)–(d), respectively, for the March 31 data. The spectra and the ratio on March 31 are binned for presentation purposes.

3.2) slope. We hence regard the single power-law model as inappropriate, both on March 27 and March 31.

Based on the above consideration, we next fitted the spectra with a model composed of a power-law component and a thermal emission component: a blackbody (bbodyrad in XSPEC terminology) or a multi-color disk blackbody (diskbb Mitsuda et al. 1984). Here  $N_H$  is assumed as  $1 \times 10^{21} \text{ cm}^{-2}$ . Then, the spectrum on March 27 has been well described by the model, with the reduced chi-squared values of  $\chi^2/\text{dof} = 60/64$  and  $\chi^2/\text{dof} = 59/64$  in the case of bbodyrad and diskbb, respectively. These values are almost the same as that obtained with a single power-law model in which  $N_H$  is left as a free parameter, while significantly smaller than that of the same model with  $N_H = 1 \times 10^{21} \text{ cm}^{-2}$ .

The XSPEC script `simftest` shows a null-hypothesis probability of  $< 10^{-6}$  in the latter case. Both models gave relatively small photon indices:  $\Gamma = 1.8 \pm 0.2$  and  $1.6^{+0.3}_{-0.7}$ , with the bbodyrad and diskbb models, respectively.

The combination of the thermal and power-law components has successfully described the spectrum on March 31 as well. The reduced chi-squared values were slightly reduced from that of the single power-law model with  $N_H = 1 \times 10^{21} \text{ cm}^{-2}$  ( $\Delta C$ -statistic  $\approx 11$  for  $\Delta\nu = 2$ ), and the residual structure above  $\approx 2 \text{ keV}$  disappeared (Fig. 3g). The probability that the improvement is only due to a random fluctuation is 0.004, according to `simftest`. The temperature of the soft thermal component became lower by a factor of  $\approx 3$ , and the apparent linear size of its emission region became larger by a factor of 8–10, than those on March 27 (see Table 1).

The soft X-ray component is most likely optically-thick thermal emission from the surface of a compact object (if it is not a black hole) or an accretion disk. The hard component, like in the present case, is often considered to originate via Comptonization of these thermal photons by a cloud of hot electrons (e.g., Done et al. 2007; Lin et al. 2007). Assuming that the observed hard tail is produced by Comptonization, we replaced the phenomenological power-law model with the `compps` model (Poutanen & Svensson 1996).

The `compps` model calculates a Comptonized spectrum when we specify the electron temperature  $kT_e$ , the optical depth for scattering  $\tau$ , the energy distribution of the seed photons, and the geometry of the Comptonization cloud (or corona). In the present study, following previous works (e.g., Sakurai et al. 2014), a spherical corona (`geom` = 4) was assumed (but see below for the cases of different geometries), with only thermal electrons. We first tested the case where the seed photons are provided by blackbody emission. The model is expressed as TBabs\*(compps+bbodyrad), where the seed photon temperature  $kT_{\text{seed}}$  of the `compps` component was linked to  $kT_{\text{bb}}$  of the bbodyrad component. Since the data did not allow us to simultaneously constrain  $\tau$  and  $kT_e$ , we fixed  $kT_e$  at 20 keV and 100 keV, and left  $\tau$  as a free parameter. The other free parameters in this model are  $kT_{\text{bb}}$  and the normalizations of the bbodyrad and `compps` components. We ignored the reflection component from the disk.

This model, TBabs\*(compps+bbodyrad), fitted the two spectra well, and yielded the best-fit parameters given in Table 1. Both spectra favored slightly smaller values of  $R_{\text{bb}}$  and  $\tau$ , if we assume  $kT_e = 100 \text{ keV}$ , compared with the case of  $kT_e = 20 \text{ keV}$ .

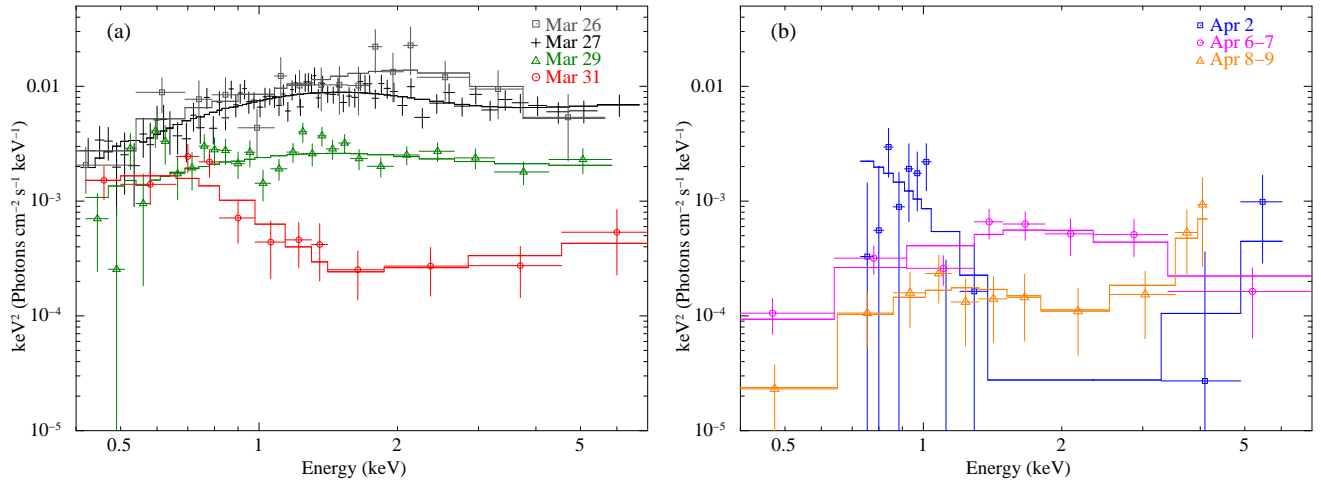


**Figure 4.** Time-averaged *Swift*/XRT spectra in the individual epochs on (a) March and (b) April, in the  $\nu F_\nu$  form, with their best-fit **TBabs\*(powerlaw+bbbodyrad)** models. The March 27 and 31 spectra in (a) are identical to those in Fig. 3.

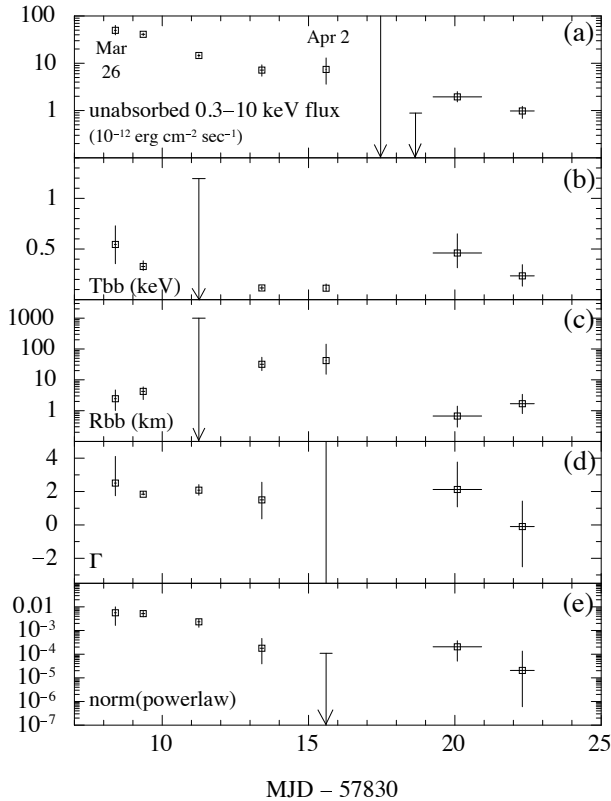


**Figure 5.** Time evolution of the parameters of the **TBabs\*(bbbodyrad+powerlaw)** model. (a) The unabsorbed 0.3–10 keV flux, (b) the temperature of the blackbody component, (c) the emission radius of the blackbody component, (d) the photon index, and (e) the normalization of the powerlaw component. The photon index on MJD 57845 (April 2) was not constrained. Only a loose flux limit ( $< 1.3 \times 10^{-8}$  erg cm $^{-2}$  s $^{-1}$ ) was obtained for MJD 57847 (April 4).

We also tested the alternative possibility that the seed photons of Comptonization are provided by disk blackbody emission. Thus, the **bbbodyrad** component

in the **TBabs\*(compps+bbbodyrad)** model was replaced by **diskbb**, and the inner disk temperature  $kT_{\text{in}}$  of **diskbb** was set to be the same as  $kT_{\text{seed}}$  of **compps** ( $kT_{\text{seed}} = -kT_{\text{in}}$ , in XSPEC terminology). This **TBabs\*(compps+diskbb)** model was also found to fit the two spectra well, yielding comparable reduced  $\chi^2$  values to those of **TBabs\*(compps+bbbodyrad)**.

Although we have assumed a spherical corona above, following previous works, we have confirmed that the choice of the coronal geometry does not affect the main conclusions from the **TBabs\*(compps+bbbodyrad)** and **TBabs\*(compps+diskbb)** models. If a slab or cylindrical corona is assumed (i.e., **geom** = 1 or 2, respectively),  $\tau$  changes by a factor of  $\lesssim 2$ , but the other free parameters remain unchanged within their 90% error ranges. The chi-squared values were also found to depend little ( $|\Delta\chi^2| \lesssim 1$ ) on the assumed coronal geometries.

We next investigated the spectral variation over a longer period. Figure 4 presents the other XRT spectra, in addition to those of March 27 and 31, which were already analyzed. The spectral profile varied in a complex manner: the peak energy of the soft component shifted toward higher energies from March 31 to April 6–7 and then moved back to lower energies in April 8–9, even though the X-ray flux was comparable among these three epochs. These XRT spectra were also well reproduced individually by the **TBabs\*(powerlaw+bbbodyrad)** model.

Figure 5 shows the best-fit parameters of these spectra in chronological order. It also shows the  $3\sigma$  upper limits of the unabsorbed 0.3–10 keV flux on April 4 and 5, calculated by assuming the best-fit model on April 6. As suggested by the spectral shape changes, the variations of  $kT_{\text{bb}}$  and  $R_{\text{bb}}$  are rather complex, and cannot be described as a simple function of the X-ray flux.

The spectra were also fit well with the TBabs\*(powerlaw+diskbb) model. The derived  $kT_{\text{in}}$  and  $R_{\text{in}}$  varied in a similar manner to  $kT_{\text{bb}}$  and  $R_{\text{bb}}$  of the TBabs\*(powerlaw+bodyrad) model, respectively.

### 3. OPTICAL OBSERVATIONS AND MULTI-WAVELENGTH SPECTRAL ENERGY DISTRIBUTIONS

Optical photometric observations of MAXI J1807+132 were performed with the  $g'$ -,  $R_C$ -, and  $I_C$ -band filters for 4 nights from 2017 March 27 to 30, with the *Murikabushi* 105 cm telescope at the Ishigakijima Astronomical Observatory in Okinawa, Japan, and the *MITSuME* 50 cm telescope of Akeno Observatory in Yamanashi, Japan (for detailed information, see Tachibana et al. 2017b, and reference therein). The target was observed for  $\sim 2$  h on each day, during which simultaneous three-band observations were repeated, with the individual exposure times of 60 s. The raw data were pre-processed in a standard manner: subtraction of dark and bias, followed by flat fielding. The pixel coordinates were calibrated into celestial coordinates via WCSTools (Mink 1997). After these treatments, we combined all the frames taken in a night in each band, and performed aperture photometry using IRAF tasks to estimate the magnitude of this object by comparing with six local reference stars. Figure 6 shows the stacked  $R_C$ -band image obtained with the *Murikabushi* telescope on March 27, where MAXI J1807+132 and the 6 reference stars are indicated.

The apparent magnitudes in the individual nights are plotted in Figure 7, which clearly shows decay in all three bands, typically by  $\sim +0.4$  mag per day. Previously, the source was much fainter, at least by  $\sim 3$  mag, because multi-epoch Pan-STARRS observations gave an average  $r$ -band magnitude of  $21.19 \pm 0.09$  mag (Denisenko 2017), which is  $\sim 3$  mag larger (i.e., the flux is  $\sim 16$  times lower) than the  $R_C$ -band magnitude estimated on March 27. This suggests that the emission from the companion star contributes only less than  $\sim 6\%$  of the total optical flux on March 27.

Figure 8 shows the multi-wavelength spectral energy distribution (SED) on March 27, where the *Swift*/XRT and UVOT data are plotted together with those from the *Murikabushi* telescope. Here we examine the optical flux for a possibility of emission from the outer region of a standard accretion disk, irradiated by X-ray emission. The illuminating source is ambiguous; either a disk blackbody emission if the central object is a black hole, or a disk blackbody plus blackbody if a neutron star. However, there is no available model that includes blackbody emission. We thus account only for the disk black-

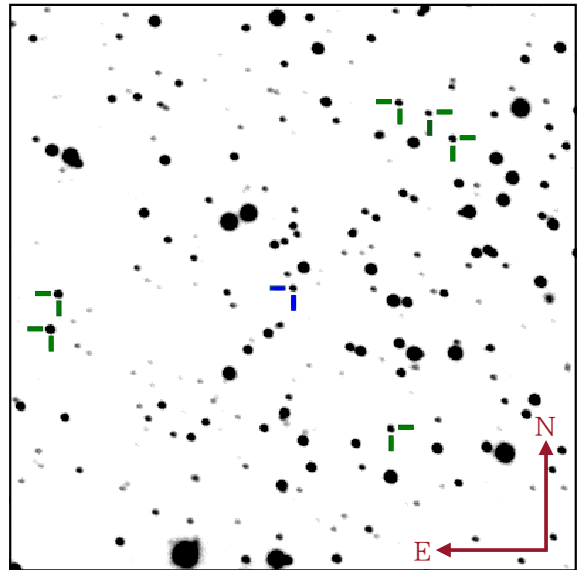


**Figure 6.** An  $R_C$ -band finding chart for MAXI J1807+132, with a field of view of  $4'.8 \times 4'.8$ . The pair of blue bars at the center of the image point MAXI J1807+132, while green bars indicate the field reference stars.

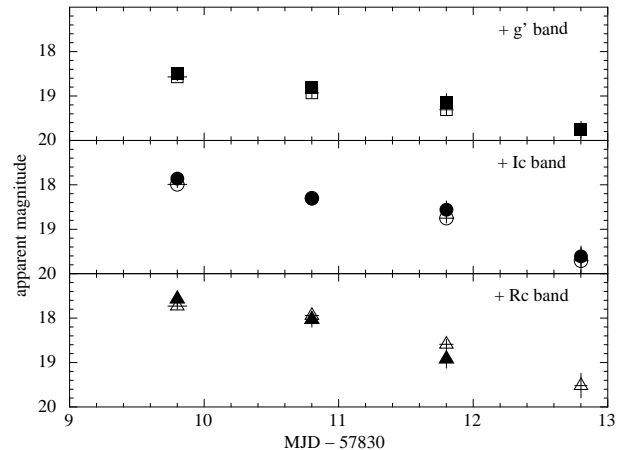


**Figure 7.** The optical light curves of MAXI J1807+132 in the  $g'$ -,  $R_C$ -, and  $I_C$ -bands. The open and filled symbols indicate the data from *Murikabushi* and *MITSuME* telescopes, respectively.

body emission here and attempt to fit the SED with an irradiated disk model “*diskir*” (Gierliński et al. 2008, 2009).

The *diskir* model calculates the emission from a standard disk, considering partial Comptonization of inner-disk photons. The outer region of the disk is assumed to be illuminated by a fraction of X-rays from the central region, to achieve a higher temperature and emissivity via reprocessing. The free parameters of the model are the inner disk temperature  $kT_{\text{in}}$ , the photon index  $\Gamma$  and electron temperature  $kT_e$  of the Comptonized com-

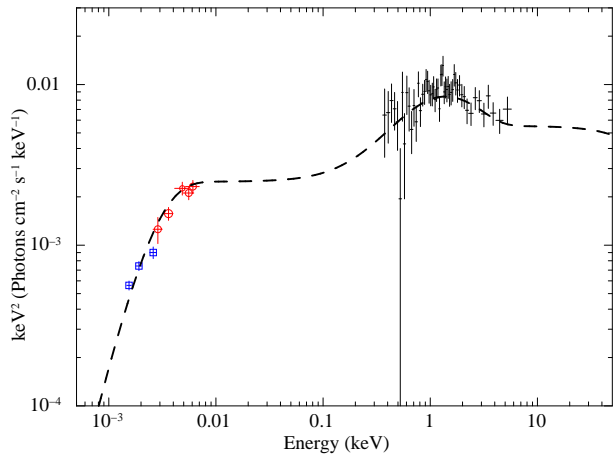


**Figure 8.** A multi-wavelength SED of MAXI J1807+132 on March 27 corrected for interstellar extinction. The *Swift*/XRT (black crosses), *Swift*/UVOT (red open circles), and the optical  $g'$ ,  $R_C$ , and  $I_C$ -band data (blue open squares) from the *Murikabushi* telescope are plotted. The dashed line shows the best-fit `diskir` model.

ponent, the luminosity ratio  $L_C/L_d$  between the Comptonized corona and the disk, the fraction  $f_{in}$  of the luminosity of the Comptonized component that is thermalized in the inner disk, the fraction  $f_{out}$  of the bolometric flux that illuminates the outer disk, the radius  $r_{irr}$  of the Compton illuminated disk, the outer disk radius  $R_{out}$ , and the normalization, depending on the inner disk radius  $R_{in}$  and the distance in the same manner as `diskbb`. Following previous works (Gierliński et al. 2008, 2009), we set  $r_{irr} = 1.1R_{in}^2$ . Considering the results of our XRT spectral analysis, we assumed  $\Gamma = 2.0$ ,  $kT_e = 100$  keV,  $f_{in} = 0.1$ , and left the other parameters free to vary. To account for the optical extinction, the `redden` model with  $E(B - V) = 0.13$  (which is converted to  $N_H \sim 1 \times 10^{21}$  cm $^{-2}$  via the relation given in Predehl & Schmitt 1995) was multiplied to `diskir`.

As shown in Figure 8, the overall SED profile has been reasonably well reproduced by the `diskir` model with  $kT_{in} \approx 0.4$  keV,  $L_C/L_d \approx 2.3$ ,  $R_{in} \approx 3$  km,  $R_{out} \approx 1 \times 10^5 R_{in} \approx 3 \times 10^5$  km (where the distance and inclination are assumed as 5 kpc and  $0^\circ$ , respectively), and  $f_{out} \approx 3.7 \times 10^{-2}$ . The estimated values of  $kT_{in}$  and  $R_{in}$  are comparable with those obtained from the XRT data alone using the `diskbb+powerlaw` model (Section 2.2).

#### 4. DISCUSSION

<sup>2</sup> We have confirmed that the choice of the  $R_{irr}$  value does not strongly affect the estimation of  $f_{out}$ . The resultant  $f_{out}$  value was kept unchanged within its 90% confidence range, in the case of  $R_{irr} = 1.1, 5, \text{ and } 10$ .

#### 4.1. The Nature of MAXI J807+132

We studied the behavior of the new X-ray transient MAXI J1807+132 using the multi-wavelength data of the MAXI/GSC, *Swift*, and optical telescopes. The source is likely to be identified with 2MAXIt J1807+132, which is listed in the first MAXI/GSC transient source catalog (Kawamuro et al. 2016) based on a long-term X-ray brightening event in 2011 May. Although Kawamuro et al. (2016) primarily aimed at a search for tidal disruption events (TDEs) by extragalactic supermassive black holes, the 2011 May episode of 2MAXIt J1807+132 was not categorized therein as a TDE. Below, we consider various interpretations of the nature of this object.

##### 4.1.1. A Tidal Disruption Event?

Kawamuro et al. (2016) concluded that 2MAXIt J1807+132 is unlikely a TDE, because it has exhibited multiple enhancements (though with lower significances, at  $\sim 2\sigma$  levels) from 2009 to 2013. Identifying the present source MAXI J1807+132 with 2MAXIt J1807+132, the TDE interpretation becomes even less likely, because the interval of the two strongest flaring events is much shorter than those predicted for TDEs (typically  $\sim 10^4$  to  $\sim 10^5$  years; e.g., Kawamuro et al. 2016).

To search for other brightening episodes of MAXI J1807+132 (=2MAXIt J1807+132), we analyzed the entire MAXI/GSC data of this sky region using the on-demand process system<sup>3</sup>. Figure 9 shows the obtained light curve, from 2009 August to 2017 April. However, we detected no X-ray enhancements with a significance of  $>3\sigma$ , other than the flares in 2011 and 2017. As noticed in Fig. 9, the present flaring event in 2017 is the brightest one in the last 7.5 years.

The *Swift*/XRT data allow us to further argue against the TDE interpretation of the present object. The XRT spectra of MAXI J1807+132 in 2017 March and April have been well described with a soft thermal component (blackbody or disk blackbody) visible below  $\sim 2$  keV, and a hard tail with a photon index of  $\sim 2$ . The thermal component has a temperature higher than those of TDEs (typically  $\lesssim 0.1$  keV; Esquej et al. 2008; Maksym et al. 2010). The hard X-ray tail is much stronger than those of non-jetted TDEs, although it could be compatible with the spectrum of the jetted TDE Swift J164449.3+573451 (Burrows et al. 2011; Bloom et al. 2011; Levan et al. 2011).

Typical TDEs, either with or without jets, are considered to decay with time  $t$  as  $\propto t^{-5/3}$  (e.g., Rees 1988;

<sup>3</sup> <http://maxi.riken.jp/mxondem/>



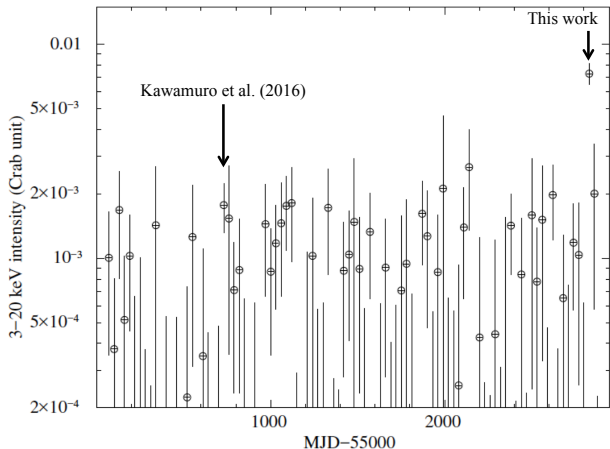


**Figure 9.** A 2–20 keV MAXI/GSC light curve of MAXI J1807+132 for the last  $\approx 7.5$  years, with 30-day time bins. The thick solid arrows indicate the flares reported by Kawamuro et al. (2016) and this work.

Phinney 1989). In contrast, the X-ray emission of MAXI J1807+132 in the present flaring event decayed much more rapidly; fitting the XRT light curve (Fig. 5a) with a power-law model, we obtained the best-fit decay curve as  $\propto t^{-6\pm 1}$ , where  $t$  is the time since 2017 March 13 when the source was first recognized with MAXI. This fast decay also shows that the source is unlikely a TDE.

#### 4.1.2. A Galactic Magnetic Cataclysmic Variable (CV)?

Having excluded the TDE interpretation, we hereafter assume that the source is a binary system located in our galaxy. One of the most abundant subclasses of such binaries is accreting magnetic CVs (Polars and Intermediate Polars). Indeed, the X-ray flux observed on March 31,  $\sim 7 \times 10^{-12}$  erg cm $^{-2}$  s $^{-1}$ , translates to a source luminosity of  $\sim 10^{34}$  erg s $^{-1}$ , if the source distance is assumed, e.g., to be 5 kpc. This luminosity is typical of magnetic CVs during their brightening episodes (e.g., Revnivtsev et al. 2008). An X-ray spectrum of a typical CV is composed of an optically thin thermal plasma emission produced in the accretion columns, and a blackbody emission from the polar cap region of the white dwarf. We found that the XRT spectra of MAXI J1807+132 above 1 keV can be fit with the optically thin plasma model `mekal` with a temperature of  $\gtrsim 5$  keV, which is consistent with those of typical magnetic CVs. However, the soft thermal component of MAXI J1807+132 has a much higher temperature than the blackbody component in CVs ( $< 0.1$  keV). Therefore, the magnetic CV interpretation is unlikely.

#### 4.1.3. A High Mass X-ray Binary (HMXB)?

Since MAXI J1807+132 is located at a relatively high Galactic latitude of  $15^\circ$ , the possibility of its being a

HMXB would be low. If the companion star was an O or B-type star located at  $\sim 8$  kpc, with an absolute  $V$ -band magnitude of  $-4$  to  $0$  mag, we should have easily detected it with an apparent magnitude of  $10$ – $15$  mag, even when the system was not active. In addition, during the present X-ray brightening, the optical flux of MAXI J1807+132 increased by an order of magnitude above the quiescence level. Such optical brightening should not take place in HMXBs even during increased mass accretion rates, because their optical fluxes are dominated by those from the mass-donating companions rather than from outer accretion disks. Finally, MAXI J1807+132 exhibited spectra that are considerably softer than those of high mass X-ray pulsars, which are roughly described by a power-law with a photon index of  $\lesssim 1$  (Coburn et al. 2002). Therefore, MAXI J1807+132 cannot be a HMXB, regardless of the nature of the compact object involved.

#### 4.1.4. A transient BHXB?

The long-term spectral variation of MAXI J1807+132 throughout the present outburst is qualitatively similar to those seen in transient BHXBs. The spectrum became softer from March 26–29 to March 31 and harder again in April. Under the limited statistics of the XRT data, this behavior could be explained if we were witnessing a hard-to-soft and soft-to-hard transitions in these periods, respectively. Therefore, below we examine in more details whether this interpretation is feasible or not.

If the source is a BHXB as assumed above, the prominent, low-temperature component seen on March 31 should be explained as disk emission in the soft state or an intermediate state (if in the hard state, the disk emission would not be as bright as in the March 31 spectrum). Indeed, similar temperature and strength of the soft component have been obtained in other BHXBs (e.g., Nakahira et al. 2014). However, if this were the case, MAXI J1807+132 should have an unusually large distance. Taking into account that the soft-to-hard transition of BHXBs normally occurs at a few % Eddington luminosity (Maccarone 2003), which corresponds to  $\sim 10^{37} (M_{\text{BH}}/10 M_\odot)$  erg s $^{-1}$  ( $M_{\text{BH}}$  being the black hole mass), the March 31 flux as quoted above ( $\sim 7 \times 10^{-12}$  erg cm $^{-2}$  s $^{-1}$ ) implies a source distance as large as  $\sim 100 (M_{\text{BH}}/10 M_\odot)^{1/2}$  kpc.

There is yet another evidence against the BHXB interpretation. Applying the `diskbb+powerlaw` model to the March 27 spectrum, we obtained an unusually small inner disk radius,  $R_{\text{in}} \sim 1 (\frac{\cos i}{\cos 0^\circ})^{-1/2} (D/5 \text{ kpc})$  km. In order to identify it with the radius of the innermost circular orbit, we would have to assume an extreme in-

clination, e.g.,  $i \gtrsim 85^\circ$ , and a very light black hole (e.g.,  $\sim 3 M_\odot$ ) with a substantial spin.

Modeling the multi-wavelength SED on March 27 with the `diskir` model (Section 3) yielded an irradiation fraction of  $f_{\text{out}} \approx 3.7 \times 10^{-2}$ . This value is about several to ten times larger than those obtained from black hole X-ray binaries with X-ray luminosities of  $\gtrsim 10^{35}$  erg s $^{-1}$  (e.g., Gierliński et al. 2008, 2009; Chiang et al. 2010; Shidatsu et al. 2013; Nakahira et al. 2014, but see Rahoui et al. 2012). Even if no extinction is assumed (where the optical flux changes only by a factor of  $\approx 2$ ), the value of  $f_{\text{out}}$  is reduced only by a factor of  $\lesssim 3$ , and is still somewhat larger than that of black hole X-ray binaries. The situation worsens if we assume the stronger reddening,  $E(B-V) = 0.28$ , estimated via optical spectroscopy (Muñoz-Darias et al. 2017). Considering all these results, we conclude that the source is unlikely to be a BHXB.

#### 4.1.5. A Neutron Star LMXB?

A remaining possibility is that the source is a neutron star LMXB. The XRT spectra resemble those of neutron star LMXBs in their dim phases, with a luminosity below  $\sim 10^{35}$  erg s $^{-1}$ ; at this luminosity range, they often exhibit a prominent soft thermal component with a power-law tail (Asai et al. 1996; Wijnands et al. 2001; Jonker et al. 2005; Sakurai et al. 2014; Chakrabarty et al. 2014), whereas such an apparent two-component feature is less significant when they are in the more luminous hard state (e.g., Barret 2001; Lin et al. 2007; Armas Padilla et al. 2017b). In particular, the properties of the XRT spectrum on 2017 March 27 are similar to those obtained in the two *Suzaku* observations of Aql X-1 in its dim phases (“Obs 5” and “Obs 6” in Sakurai et al. 2014), as noticed by comparing the `compps` results. If MAXI J1807+132 is a neutron star LMXB, and if the unabsorbed 0.8–100 keV luminosity on March 27 was between those in “Obs 5” and “Obs 6” of Aql X-1 ( $5 \times 10^{35}$  erg s $^{-1}$  and  $1 \times 10^{34}$  erg s $^{-1}$ , respectively), the distance is calculated as  $D \sim 1$ –8 kpc.

A similar distance,  $D = 5$  kpc, is derived from the relation between the luminosity versus the photon index for neutron star LMXBs (Wijnands et al. 2015), by using the photon index on March 27 ( $\Gamma \approx 2.4$ , when a single power-law model is applied) and the unabsorbed flux,  $4 \times 10^{-11}$  erg cm $^2$  sec $^{-1}$ . Assuming  $D = 5$  kpc, the  $3\sigma$  upper limit of the unabsorbed 0.3–10 keV flux on April 5,  $8.8 \times 10^{-13}$  erg cm $^{-2}$  s $^{-1}$ , which is the lowest flux constraint in the XRT datasets, is converted to the Eddington ratio of  $\approx 1.5 \times 10^{-5}$ , for a neutron star with a mass of  $1.4 M_\odot$ . This value is consistent with the min-

imum luminosity for neutron star LMXBs determined by Tomsick et al. (2005).

Such a low luminosity (below  $10^{35}$  erg s $^{-1}$ ) would be favored to explain the high  $L_{\text{OPT}}/L_X$  ratio, where  $L_{\text{OPT}}$  and  $L_X$  are the optical and X-ray luminosities, respectively, given a correlation of  $L_{\text{OPT}} \propto L_X^\alpha$  with  $\alpha \sim 0.5$  (van Paradijs & McClintock 1994; Russell et al. 2006, 2007). The X-ray flux of MAXI J1807+132 decreased by  $\sim 2$  orders of magnitude from March 26 to the early April. Similar rapid flux decay has been observed in other neutron star LMXBs, such as Aql X-1, 4U 1608–52, and MAXI J1421–613 (Campana et al. 1998; Asai et al. 2013; Serino et al. 2015), at luminosities below  $10^{36}$  erg s $^{-1}$ , where the propeller effect is considered to start operating, and the centrifugal force prevents steady accretion onto the neutron star (Matsuoka & Asai 2013). These results provide yet another support to our identification of MAXI J1807+132 with a neutron star LMXB in a dim phase.

#### 4.2. Physical Interpretation of the X-ray Spectra and Their Variations

Let us examine the X-ray properties of MAXI J1807+132, assuming that it is a dim neutron star LMXB. The soft X-ray component of such an object, at luminosities below  $\sim 10^{35}$  erg s $^{-1}$ , is generally considered as thermal emission from the surface of the neutron star. The small radius of the blackbody emission region (a few km) can be naturally explained if only a part of the surface radiates X-rays. In fact, the blackbody radius of Aql X-1 was found to decrease from  $\sim 10$  km at  $\sim 1 \times 10^{36}$  erg s $^{-1}$  down to  $\sim 3$  km at  $\sim 1 \times 10^{34}$  erg s $^{-1}$  (Figure 6 of Sakurai et al. 2014), presumably because of the appearance of weak magnetic fields which limit the accretion flows to the magnetic poles. By contrast, the origin of the hard power-law tail is not yet fully understood. It allows several different interpretations, such as Comptonization of the blackbody emission in a hot accretion flow (Sakurai et al. 2014), bremsstrahlung from the hot flow itself (Chakrabarty et al. 2014), and the jet emission (Fender et al. 2003). In Section 2.2, we applied the `compps` model to the XRT spectra on March 27 and 31, to examine the first interpretation in comparison with the *Suzaku* results of Aql X-1 (Sakurai et al. 2014), and found similarities in their best-fit parameters (see also Section 4.1.5).

The contribution by bremsstrahlung from the Comptonized corona was evaluated quantitatively by Ono et al. (2017), based on the observationally estimated accretion flow geometry in Aql X-1. When the source luminosity is  $> 5 \times 10^{36}$  erg s $^{-1}$ , they estimated that the bremsstrahlung luminosity is  $L_{\text{Br}} \sim 1 \times 10^{34}$  erg s $^{-1}$ .

Then, assuming that MAXI J1807+132 has a typical luminosity of  $2 \times 10^{35}$  erg s $^{-1}$ , and that  $L_{\text{Br}}$  decreases as the mass accretion rate gets lower, we conclude that  $L_{\text{Br}}$  is likely to be still lower than the luminosity of the power-law tail.

We have detected significant variations in the temperature and the radius of the emission region of the blackbody component, which are not determined by the X-ray luminosity alone (see Fig. 4 and Fig. 5). Similar peculiar behavior has been observed in other LMXBs, like Aql X-1 (Rutledge et al. 2002) and XTE J1709–267 (Jonker et al. 2005), at luminosities of  $10^{33}$ – $10^{35}$  erg s $^{-1}$ . These variations were suggested to arise from residual accretion onto the polar-cap region of the neutron star, in association with neutron star cooling (e.g., Cackett et al. 2010; Degenaar & Wijnands 2012). In the case of MAXI J1807+132, however, it is unclear whether the neutron star was at the stage of crustal cooling during the *Swift* observations, provided that the timescale of its flux decay was somewhat shorter than those in other neutron star LMXBs in quiescence (Homan et al. 2015).

The spectra of MAXI J1807+132 could be categorized into two types: (1) a flatter profile with a higher  $kT_{\text{bb}}$  and a smaller  $R_{\text{bb}}$  (e.g., the March 27 spectrum), and (2) a more complex profile in which the soft component, with a lower  $kT_{\text{bb}}$  and a larger  $R_{\text{bb}}$ , and the hard tail are distinctive (e.g., the March 31 spectrum). This bimodality cannot be attributed to luminosity changes, since the spectrum switched a few times between the two types as the overall X-ray luminosity decayed almost monotonically.

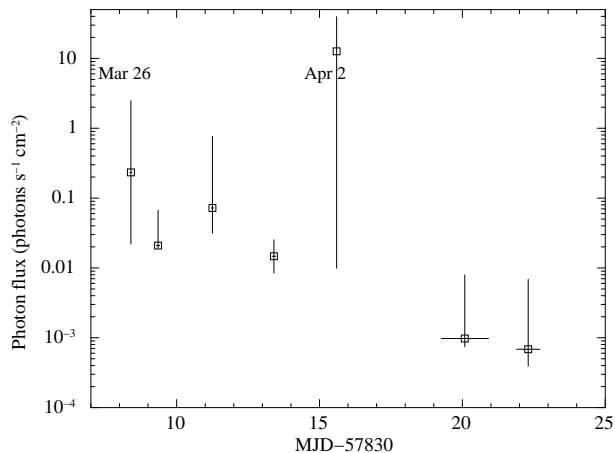


**Figure 10.** Variation of the 0.01–100 keV photon flux of the soft thermal emission, calculated with the `tbabs*(bbodyrad+compps)` model. The abscissa is the same as Fig. 5.

One possible explanation of the observed variations between the two types would be to assume that the seed blackbody spectrum suffers strong color hardening, by a factor of  $\kappa \sim 3$ , in type-(1) spectra, whereas such an effect is small in type-(2) spectra so that the seed spectrum is close to a “bare” blackbody. In fact, Takahashi et al. (2009) observed spontaneous fluctuations in  $\kappa$  in the LMXB 4U 1608–52 (even though the effect was only  $\sim 20\%$  and was observed in the disk emission of the soft state). To examine this interpretation, we investigated the trend in the total photon flux of the soft thermal component, including both the direct and Compton-scattered components, assuming isotropic emission and conservation of the number of photons in Comptonization. In this analysis, the `TBabs*(bbodyrad+compps)` model was applied to the individual XRT spectra with  $kT_e = 100$  keV. As shown in Figure 10, the photon flux decreased rather monotonically. Thus, the observed variations could be described by a change in the color hardening factor (for some unspecified reasons) during a monotonic decrease in the mass accretion rate.

#### 4.3. X-ray and Optical Flux Correlation

The optical flux was reduced from March 27 to 31 by  $\sim 0.4$  mag per day as the X-ray flux decreased. The optical decay can be expressed as  $F_{\text{OPT}} \propto \exp(-t/\beta_{\text{OPT}})$ , where  $F_{\text{OPT}}$  represents the optical flux and  $\beta_{\text{OPT}} \sim 2.7$  day. Fitting the XRT 0.3–10 keV light curve (Fig. 5) in March 26–31 with an exponential function,  $F_X \propto \exp(-t/\beta_X)$ , we obtain  $\beta_X = 2.4 \pm 0.5$ . From these two functions, the X-ray versus optical flux relation is derived as  $F_{\text{OPT}} \propto F_X^\alpha$ , where  $\alpha \sim 0.7$ – $1.1$ . This  $\alpha$  value is comparable with those obtained for other neutron star LMXBs in their dim ( $L_X \lesssim 10^{36}$  erg s $^{-1}$ ) periods (van Paradijs & McClintock 1994; Russell et al. 2006, 2007), which have been explained by reprocessing of X-ray irradiation in the outer accretion disk. We also find that the optical and X-ray luminosities on March 27, estimated by assuming a distance of 5 kpc, lie on the trend in  $L_X$  and  $L_{\text{OPT}}$  of neutron star LMXBs in Russell et al. (2007). These results further reinforce the LMXB interpretation of MAXI J1807+132.

We are grateful to the anonymous referee for constructive comments. MS acknowledges support by the Special Postdoctoral Researchers Program at RIKEN. This work is partly supported by a Grant-in-Aid for Young Scientists (B) 16K17672 (MS), for JSPS Fellows for young researchers (YT, TK), and for Scientific Research 17K05384 (YU) and 16K05301 (HN). This research has made use of MAXI data provided by RIKEN,

JAXA and the MAXI team and *Swift* data supplied by the UK Swift Science Data Centre at the University of Leicester. This work was partially carried out by the

joint research program of the Institute for Cosmic Ray Research (ICRR), University of Tokyo.

*Facilities:* MAXI (GSC), Swift (XRT, UVOT)

*Software:* UK Swift Science Data Centre tools (Evans et al. 2009), HEASOFT, XSPEC (Arnaud 1996)

## REFERENCES

- Armas Padilla, M., Wijnands, R., Degenaar, N., et al. 2017a, *The Astronomer's Telegram*, #10224
- Armas Padilla, M., Ueda, Y., Hori, T., Shidatsu, M., & Muñoz-Darias, T. 2017b, *MNRAS*, 467, 290
- Arnaud K. A., 1996, *adass V*, 191, 17
- Asai, K., Dotani, T., Mitsuda, K., et al. 1996, *PASJ*, 48, 257
- Asai, K., Matsuoka, M., Mihara, T., et al. 2013, *ApJ*, 773, 117
- Barret, D. 2001, *Adv. Space Res.*, 28, 307
- Bloom, J. S., Giannios, D., Metzger, B. D., et al. 2011, *Science*, 333, 203
- Burrows, D. N., Kennea, J. A., Ghisellini, G., et al. 2011, *Nature*, 476, 421
- Cackett, E. M., Brown, E. F., Miller, J. M., & Wijnands, R. 2010, *ApJ*, 720, 1325
- Campana, S., Stella, L., Mereghetti, S., et al. 1998, *ApJL*, 499, L65
- Cash, W. 1979, *ApJ*, 228, 939
- Chakrabarty, D., Tomsick, J. A., Grefenstette, B. W., et al. 2014, *ApJ*, 797, 92
- Chiang, C. Y., Done, C., Still, M., & Godet, O. 2010, *MNRAS*, 403, 1102
- Coburn, W., Heindl, W. A., Rothschild, R. E., et al. 2002, *ApJ*, 580, 394
- Degenaar, N., & Wijnands, R. 2012, *MNRAS*, 422, 581
- Denisenko, D. 2017, *The Astronomer's Telegram*, #10217
- Done, C., Gierliński, M., & Kubota, A. 2007, *A&A Rv*, 15, 1
- Esquej, P., Saxton, R. D., Komossa, S., 2008, *A&A*, 489, 543
- Evans, P. A., Beardmore, A. P., Page, K. L., et al. 2009, *MNRAS*, 397, 1177
- Fender, R. P., Gallo, E., & Jonker, P. G. 2003, *MNRAS*, 343, L99
- Gehrels, N., Chincarini, G., Giommi, P., et al. 2005, *ApJ*, 621, 558
- Gierliński, M., Done, C., & Page, K. 2008, *MNRAS*, 388, 753
- Gierliński, M., Done, C., & Page, K. 2009, *MNRAS*, 392, 1106
- Homan, J., Fridriksson, J. K., Wijnands, R., et al. 2015, *ApJ*, 795, 131
- Jonker, P. G., Galloway, D. K., McClintock, J. E., et al. 2005, *MNRAS*, 354, 666
- Kawamuro, T., Ueda, Y., Shidatsu, M., et al. 2016, *PASJ*, 68, 58
- Kennea, J. A., Evans, P. A., Beardmore, A. P., et al. 2017a, *The Astronomer's Telegram*, #10215
- Kennea, J. A., Siegel, M. H., Evans, P. A., et al. 2017b, *The Astronomer's Telegram*, #10216
- Kong, A. K. H., Jin, R., Tseng, C.-H., & Lin, E.-T. 2017, *The Astronomer's Telegram*, #10245
- Levan, A. J., Tanvir, N. R., Cenko, S. B., et al. 2011, *Science*, 333, 199
- Lin, D., Remillard, R. A., & Homan, J. 2007, *ApJ*, 667, 1073
- Maccarone, T. J. 2003, *A&A*, 409, 697
- Maksym, W. P., Ulmer, M. P., & Eracleous, M. 2010, *ApJ*, 722, 1035
- Matsuoka, M., Kawasaki, K., Ueno, S., et al. 2009, *PASJ*, 61, 999
- Matsuoka, M., & Asai, K. 2013, *PASJ*, 65, 26
- Mihara, T., Nakajima, M., Sugizaki, M., et al. 2011, *PASJ*, 63, 623
- Mitsuda, K., Inoue, H., Koyama, K., et al. 1984, *PASJ*, 36, 741
- Mink, D. J., 1997, *Astronomical Society of the Pacific Conference Series*, 125, 249
- Morii, M., Yamaoka, H., Mihara, T., Matsuoka, M., & Kawai, N. 2016, *PASJ*, 68, 11
- Muñoz-Darias, T., Jimenez-Ibarra, F., Mata Sanchez, D., et al. 2017, *The Astronomer's Telegram*, #10221
- Nakahira, S., Negoro, H., Shidatsu, M., et al. 2014, *PASJ*, 66, 84
- Negoro, H., Kohama, M., Serino, M., et al. 2016, *PASJ*, 68, 1
- Negoro, H., Kawamuro, T., Ueda, Y., et al. 2017, *The Astronomer's Telegram*, #10208
- Ono, K., Makishima, K., Sakurai, S., et al. 2017, *PASJ*, 69, 23

- Phinney, E. S. 1989, *The Center of the Galaxy*, 136, 543
- Poutanen, J., & Svensson, R. 1996, *ApJ*, 470, 249
- Predehl, P., & Schmitt, J. H. M. M. 1995, *A&A*, 293, 889
- Rahoui, F., Coriat, M., Corbel, S., et al. 2012, *MNRAS*, 422, 2202
- Rees, M. J. 1988, *Nature*, 333, 523
- Revnivtsev, M., Sazonov, S., Krivonos, R., Ritter, H., & Sunyaev, R. 2008, *ApJ*, 489, 1121
- Roming, P. W. A., Kennedy, T. E., Mason, K. O., et al. 2005, *SSRv*, 120, 95
- Russell, D. M., Fender, R. P., Hynes, R. I., et al. 2006, *MNRAS*, 371, 1334
- Russell, D. M., Fender, R. P., & Jonker, P. G. 2007, *MNRAS*, 379, 1108
- Rutledge, R. E., Bildsten, L., Brown, E. F., Pavlov, G. G., & Zavlin, V. E., 2002, *ApJ*, 577, 358
- Sakurai, S., Torii, S., Noda, H., et al. 2014, *PASJ*, 66, 10
- Serino, M., Shidatsu, M., Ueda, Y., et al. 2015, *PASJ*, 67, 30
- Shidatsu, M., Ueda, Y., Nakahira, S., et al. 2013, *ApJ*, 779, 26
- Shidatsu, M., Tachibana, Y., Yoshii, T., et al. 2017, *The Astronomer's Telegram*, #10222
- Shields, J., Stanek, K. Z., Kochanek, C. S., et al. 2017, *The Astronomer's Telegram*, #10227
- Tachibana, Y., Yoshii, T., Shidatsu, M., et al. 2017a, *The Astronomer's Telegram*, #10223
- Tachibana, Y., Yoshii, T., Hanayama, H., & Kawai, N. 2017b, *PASJ*, 69, 63
- Takahashi, H., Sakurai, S., & Makishima K. 2009, *ApJ*, 738, 62
- Tomsick, J. A., Gelino, D. M., & Kaaret, P. 2005, *ApJ*, 635, 1233
- van Paradijs, J., & McClintock, J. E. 1994, *A&A*, 290, 133
- Wijnands, R., Miller, J. M., Markwardt, C., et al. 2001, *ApJL*, 560, L159
- Wijnands, R., Degenaar, N., Armas Padilla, M., et al. 2015, *MNRAS*, 454, 1371
- Wilms, J., Allen, A., & McCray, R. 2000, *ApJ*, 542, 914